

RESEARCH

Open Access



Patient-specific modeling of stroma-mediated chemoresistance of pancreatic cancer using a three-dimensional organoid-fibroblast co-culture system

Sebastian Schuth^{1†}, Solange Le Blanc^{1,2,3,4†}, Teresa G. Krieger^{5†}, Julia Jabs^{6,7†}, Miriam Schenk¹, Nathalia A. Giese¹, Markus W. Büchler¹, Roland Eils^{5,6}, Christian Conrad^{5,6*†} and Oliver Strobel^{1,3,4*†}

Abstract

Background Cancer-associated fibroblasts (CAFs) are considered to play a fundamental role in pancreatic ductal adenocarcinoma (PDAC) progression and chemoresistance. Patient-derived organoids have demonstrated great potential as tumor avatars for drug response prediction in PDAC, yet they disregard the influence of stromal components on chemosensitivity.

Methods We established direct three-dimensional (3D) co-cultures of primary PDAC organoids and patient-matched CAFs to investigate the effect of the fibroblastic compartment on sensitivity to gemcitabine, 5-fluorouracil and paclitaxel treatments using an image-based drug assay. Single-cell RNA sequencing was performed for three organoid/CAF pairs in mono- and co-culture to uncover transcriptional changes induced by tumor-stroma interaction.

Results Upon co-culture with CAFs, we observed increased proliferation and reduced chemotherapy-induced cell death of PDAC organoids. Single-cell RNA sequencing data evidenced induction of a pro-inflammatory phenotype in CAFs in co-cultures. Organoids showed increased expression of genes associated with epithelial-to-mesenchymal transition (EMT) in co-cultures and several potential receptor-ligand interactions related to EMT were identified, supporting a key role of CAF-driven induction of EMT in PDAC chemoresistance.

[†]Sebastian Schuth, Solange Le Blanc, Teresa G. Krieger, Julia Jabs these authors contributed equally and share first authorship.

[†]Christian Conrad and Oliver Strobel these authors contributed equally and share senior authorship.

*Correspondence:

Christian Conrad
christian.conrad@charite.de

Oliver Strobel
oliver.strobel@meduniwien.ac.at

Full list of author information is available at the end of the article



Conclusions Our results demonstrate the potential of personalized PDAC co-cultures models not only for drug response profiling but also for unraveling the molecular mechanisms involved in the chemoresistance-supporting role of the tumor stroma.

Keywords Pancreatic cancer, Patient-derived organoids, Cancer-associated fibroblasts, Drug screening, Personalized oncology

Background

Pancreatic ductal adenocarcinoma (PDAC) has become the third and fourth leading cause of cancer related death in Northern America and Europe, respectively [1]. Chemoresistance represents a major challenge in the treatment of resectable and unresectable PDAC, yet systemic therapies remain largely restricted to conventional cytotoxic drugs administered as single agents or combination regimens [2]. The PDAC tumor microenvironment, consisting mostly of extracellular matrix (ECM), cancer-associated fibroblasts (CAFs), infiltrating immune cells and vasculature, plays a crucial role in driving tumor chemoresistance via diverse, not yet fully elucidated mechanisms [3]. A very prominent desmoplastic reaction driven by CAFs constitutes up to 90% of the total PDAC tumor volume [4]. This vast tumor ECM forms a physical barrier that can lead to decreased drug delivery to tumor cells [5, 6]. Several studies suggest that CAFs promote tumor progression, metastasis and therapy resistance [7]. CAF-mediated chemoprotection against gemcitabine in PDAC is thought to involve a variety of mechanisms such as induction of anti-apoptosis/pro-survival pathways in tumor cells [8, 9], alteration of tumor gemcitabine metabolism [10, 11] and release of exosomes [12].

Suboptimal tumor modeling neglecting tumor-stromal interactions is regarded as an important contributor to the high drug attrition rate of preclinically promising drugs [13]. Incorporation of stromal components into drug screening models is therefore urgently needed. PDAC tumor organoids [14] have emerged in recent years as 3D in vitro disease models able to retain the intrinsic heterogeneity and genetic alterations of the original tumors [15–17]. As PDAC organoids are amenable to clinical application and seem to reflect patient drug response [16, 18, 19], they hold great potential for personalized oncology. Yet, drug screening based on purely epithelial organoid culture models fails to consider the contribution of the patient-specific tumor microenvironment. Hence, incorporation of relevant stromal compartments to organoid cultures is a crucial step for optimization of tumor tissue modeling and drug response prediction.

Recently, heterocellular organoid cultures have aided to grasp CAF heterogeneity and dissect complex tumor-stroma interactions. For instance, two distinct yet plastic

CAF subtypes, namely myofibroblastic and inflammatory CAFs, were identified using a murine organoid co-culture system [20]. Tsai and colleagues established cultures of PDAC organoids including CAFs and T cells, further demonstrating the suitability of these models for investigating the PDAC tumor microenvironment [21]. However, personalized drug screening assays using matched 3D heterotypic organoid cultures have not been reported yet.

Here, we established direct 3D co-culture models of patient-derived PDAC organoids (PDOs) and patient-matched CAFs. Using the live image-based drug assay DeathPro [22], we investigated the effect of CAFs on PDO chemosensitivity to the first-line chemotherapeutic drugs gemcitabine, 5-fluorouracil (5-FU) and paclitaxel, and elucidated transcriptional changes induced by tumor-stroma interaction at the single-cell level.

Methods

PDAC tumor specimens

Tumor tissue biopsies were obtained from surgically resected tumor specimens from patients who underwent primary resection at the Department of General, Visceral and Transplantation Surgery, Heidelberg University Hospital. The study was approved by the ethical committee of University of Heidelberg (ethic votes 301/2001, 159/2002, S-206/2011, S-708/2019 and S-083/2021) and was conducted in accordance with the Helsinki Declaration. All patients provided written informed consent prior to acquisition of tissue. Tumor entity was confirmed by pathological assessment of the resected specimens.

Establishment and culture of PDAC tumor organoids

Primary tumor organoid cultures were established as described previously [16]. Briefly, tumor specimens were minced and incubated in tissue digestion medium containing Advanced DMEM/F-12 (Gibco), 200 mM GlutaMAX (Gibco), 1 M HEPES (Gibco), 1x Primocin (InvivoGen), 1 mg/ml collagenase IV (Sigma-Aldrich), 100 µg/ml DNase I (AppliChem), 1x B27 (Gibco), 1 mM N-acetylcysteine (Sigma-Aldrich) and 10 µM Y-27632 (Selleckchem). Cells were resuspended in growth factor reduced Matrigel (Corning) and were seeded as 50 µl drops in 12-well plates. After 15 minutes at 37°C, 1 mL of organoid growth medium containing

Advanced DMEM/F12, 200 mM GlutaMAX, 1 M HEPES, 1x B27 supplement, 1 mM N-acetylcysteine, 10% RSPO1-conditioned medium, 100 ng/ml FGF-10 (PeproTech), 100 ng/ml Noggin (PeproTech), 500 nM A83-01 (Tocris) and 1x Primocin was added. Organoids were passaged approximately every 7 days by dissociation using TrypLE (Gibco) for 10 min at 37°C. In order to rule out overgrowth of normal ductal cells and confirmed cancer cell origin, genomic alteration profiles consistent with PDAC were verified for the established organoid lines by whole-genome sequencing as described previously in detail [16]. The success rate of tumor organoid establishment was 50%. All organoid lines were tested negative for mycoplasma contamination (Venor GeM Classic, Minerva Biolabs).

Isolation and culture of cancer-associated fibroblasts

Primary cancer-associated fibroblasts were isolated from the tumor specimens using the outgrowth method [23]. Pieces of minced tissue generated in the process of organoid isolation were separated and incubated with fibroblast medium containing RPMI Medium 1640 (Gibco) supplemented with 10% fetal calf serum (Gibco), 200 mM GlutaMAX (Gibco) and Penicillin/Streptomycin (Gibco). Success rate for CAF culture establishment was 90%. CAFs were passaged approximately every 8-9 days and their identity was confirmed by morphological assessment and immunofluorescence staining for α -SMA. All CAF lines tested negative for mycoplasma contamination and were used for experiments within 4 to 7 passages after isolation.

3D co-culture of tumor organoids and CAFs

Organoids were digested into single cells/small aggregates (organoid forming units) using TrypLE Express (Gibco) supplemented with 100 μ g/ml DNase I (AppliChem) and 10 μ M Y-27632. Organoid forming units and fibroblasts were mixed in a 1:1 ratio. Depending on the growth rate of each organoid line, 2000-3000 organoid forming units per 10 μ l of matrix was used. Cells were seeded as drops in co-culture matrix containing Matrigel and a 3 mg/ml Collagen I (Corning) gel solution mixed in a 2:1 ratio. Co-cultures were maintained in co-culture medium containing Advanced DMEM/F12, 200 mM GlutaMAX, 1 M HEPES, 1x B27, 100 ng/ml FGF-10, 50 ng/ml EGF (PeproTech) and 5% RSPO1-conditioned medium.

Image-based drug testing and drug response analysis

Chemosensitivity of organoids in mono- and co-culture was assessed using the live image-based drug assay DeathPro [22]. Mono- and co-cultures of PDOs and PDO/CAFs were seeded into μ -Chamber Angiogenesis 96-well-plates (ibidi) as 10 μ l drops in co-culture matrix

and cultured with 70 μ l co-culture medium. CAFs were stained with Cell Tracker Green CMFDA (Invitrogen) before seeding to distinguish them from PDOs. The drug screen included gemcitabine (Selleckchem), 5-FU (Selleckchem) and paclitaxel (Selleckchem). For drug treatment, serial dilutions (1:4 for gemcitabine and 5-FU, 1:3 for paclitaxel) were prepared by mixing stock solutions with co-culture medium. Drugs were applied 3 days after seeding and washed out after 72 hours. Each PDO line was tested twice independently. Confocal imaging was performed 0 and 120 h after drug application at similar positions. Four hours prior to each imaging cells were stained with 1 μ g/ml Hoechst (Invitrogen) and 1 μ g/ml propidium iodide (Sigma-Aldrich). Images were taken in a standardized way according to DeathPro image acquisition [22] using the Visual Basic for Applications macro "Autofocus Screen" [24]. Hoechst and propidium signals were acquired simultaneously, cell tracker signals sequentially to avoid spectral overlaps. Two positions were imaged per well. At each imaging position stacks of 17-18 slices with 50 μ m slice distance were acquired. Overall, approximately 90.000 confocal images were acquired, from which around 5.700 maximum intensity projections were created and analyzed. Image processing and drug response analysis was performed using the DeathPro workflow as previously described [22]. Mean values of each independent replicate were used for the analysis.

Single cell RNA-sequencing

Single cell RNA-sequencing (scRNA-seq) was performed for 3 pairs of matched PDOs/CAFs co-cultures and the corresponding PDO and CAF 3D monocultures. For each condition, 3 co-culture matrix drops of 30 μ l were seeded into one well of a 12-well plate. Single cell dissociation was performed after 5 days in culture as we previously described [25]. Single-cell sequencing libraries were prepared according to the 10x Genomics Single Cell 3 v2 Reagent Kit User Guide. Libraries were sequenced in one lane per sample with the Illumina NextSeq 500 system in high-output mode (paired-end, 75 bp).

Analysis of scRNA-seq data

Raw sequencing data were processed with CellRanger version 2.1.1 (10x Genomics), using the 10x reference human genome hg19 1.2.0 for alignment. Seurat version 3.0 [26] was used for quality control and downstream analysis. Cells with fewer than 200 genes, as well as genes represented in fewer than 3 cells, were excluded from the analysis. We also determined a maximum number of counts per gene, and a maximum fraction of mitochondrial reads, for each sample based on individual sample quality (Supplementary

Fig. 2B, Supplementary Table S1). Count data was log-normalized with a scale factor of 10,000, and the 2,000 most variable genes were identified using the FindVariableFeatures function in Seurat. Normalized data were scaled with the ScaleData function.

To differentiate CAF and PDAC cells, expression data from all samples was merged and cells were assigned their identity based on established marker genes [27]; decorin (DCN) and lumican (LUM) expression was used to identify CAFs while expression of keratin 18 (KRT18) and keratin 19 (KRT19) was used to identify tumor organoid cells. For further analysis, PDAC and CAF cells, respectively, from monoculture and co-culture samples were combined using the IntegrateData function in Seurat. Dimensional reduction was performed using the umap-learn package [28]. Cells were clustered by the Louvain algorithm with a resolution of 0.2. Differentially expressed genes were identified using a Wilcoxon rank sum test. To link differentially expressed genes with biological pathways and functions, gene set enrichment analysis was performed using the MSigDB database [29, 30], excluding genes with an adjusted p -value >0.05 . In the CAF samples, two clusters that showed enrichment for ribosomal and mitochondrial genes, respectively, were excluded from further analyses.

To distinguish iCAF-like and myCAF-like cells, we performed principal component analysis on the expression of iCAF and myCAF marker genes [27] in CAF cells, followed by Louvain clustering with a resolution of 0.1 to obtain two clusters. Scores for different gene sets were calculated using the AddModuleScore function in Seurat, using published lists of PDAC subtype marker genes [31] and gene sets from the MSigDB database [29, 30] for EMT (HALLMARK_EPITHELIAL_MESENCHYMAL_TRANSITION) and proliferation (HALLMARK_E2F_TARGETS). Cell cycle scores were calculated with the CellCycleScoring function in Seurat. Potential ligand-receptor interactions between CAF and PDAC cells in co-culture were identified using CellPhoneDB [32]; PDAC clusters 2 and 4, which

both comprised cycling cells, were combined for this analysis.

Immunofluorescence staining

Paraffin embedded tumor tissue sections of 4 μ m were co-stained with an anti-CD44 polyclonal rabbit antibody (1:150; Sigma-Aldrich, HPA005785) and an anti-HGF monoclonal mouse antibody (1:150; OriGene TA807186) overnight at 4 °C after antigen retrieval at pH8.5. Donkey anti-mouse Alexa Fluor 555 and donkey anti-rabbit Alexa Fluor 488 conjugated antibodies were incubated at 1:200 for 1 h at room temperature. Slides were mounted using Fluoroshield with DAPI (Sigma-Aldrich). Confocal images were acquired in a Nikon confocal microscope using a 60 \times oil objective. Image processing was performed in Fiji (ImageJ).

Results

3D co-cultures of matched patient-derived pancreatic tumor organoids and cancer-associated fibroblasts

Five patient-matched pairs of PDAC tumor organoids (PDAC-PDOs) and CAFs were established from surgically resected tumor samples at a success rate of 50%, with individual success rates of 50 and 93% for PDOs and CAFs, respectively. Expansion of PDOs of sufficient purity and biomass for downstream applications was completed approximately between 20 and 90 days, with a median of around 40 days. The clinicopathological characteristics of the patients are described in Table 1.

For all five PDO/CAF pairs, we established direct 3D co-culture models (Fig. 1A). For this, matched organoids and CAFs were combined at a 1:1 ratio and were cultured in a 3D matrix composed of Matrigel and collagen I. Direct physical contact of organoids and CAFs was confirmed by fluorescence staining (Fig. 1B). In line with extensive evidence that CAFs promote proliferation of tumor cells in 3D culture models [34], we observed an enhancing effect of CAFs on PDAC organoid proliferation in 4 out of 5 matched co-cultures (Fig. 1C).

Table 1 Clinicopathological characteristics of the cases and PDO subtype

Organoid line	Sex	Age (years)	Tumor type	Presentation	Tumor location	pT	pN	cM	Grading	Subtype ^a
100PO	Female	70.1	PDAC	Primary	Head	T2	N2	M0	G3	Basal-like
107PO	Male	62.6	PDAC	Primary	Head	T3	N2	M0	G2	Basal-like
112PO	Male	65.1	PDAC	Primary	Body	T3	N1	M0	G3	Classical
121PO	Female	75.3	PDAC	Primary	Body	T2	N2	M0	G2	Classical
125PO	Female	80.2	PDAC	Primary	Head	T2	N2	M0	G3	Basal-like

^a Determined from bulk RNAseq data of PDOs using PurlST [33]

Cancer-associated fibroblasts increase drug resistance of patient-matched pancreatic tumor organoids

To assess the impact of patient-matched CAFs on chemosensitivity of tumor organoids, we used the image-based drug assay DeathPro [22], which allows to evaluate independently drug-induced cell death and proliferation inhibition (PI, Fig. 1D). Sensitivity of PDOs to three chemotherapeutic drugs frequently used in the clinical treatment of PDAC, i.e., gemcitabine, 5-FU and paclitaxel, was evaluated for PDO mono- and PDO/CAF co-cultures. To discriminate CAFs from organoids in the confocal images generated by the DeathPro workflow, CAFs were stained with a cell tracker before setting up the co-cultures (Fig. 1D). By overlaying Hoechst, propidium iodide and the cell tracker signals, individual dose response curves for organoids and CAFs were generated (Fig. 1F).

We observed high reproducibility of the response curves (Supplementary Fig. S1A) and strong correlations (Pearson $R > 0.78$) for death (AUC, max. death) and proliferation inhibition (AUC_{pi}, max. PI) parameters between independent replicates (Supplementary Fig. S1B). Hoechst and propidium iodide staining had no cytotoxic effects on PDOs or CAFs (Supplementary Fig. S1C and D). In control conditions without drug treatment, the enhancing effect of CAFs on organoid proliferation resulted in an average of 1.3-fold increase in relative growth of organoids in co-culture compared to monoculture ($P < 0.05$; Fig. 1C). Basal levels of cell death in organoids under control conditions did not significantly differ between mono- and co-culture (Supplementary Fig. S1E).

Cell death induced by gemcitabine, 5-FU and paclitaxel treatments was significantly higher in PDO monocultures than in PDO/CAF co-cultures (Fig. 2A and B). Both AUC and max. Death values were on average significantly lower in co-culture conditions, indicating that the presence of CAFs resulted in increased resistance of organoids to the cytotoxic effects of chemotherapy treatments. The extent of this effect was, however, patient and drug specific, suggestive of heterogeneity in the impact of tumor-stroma interactions on chemoresistance mechanisms. PDOs in co-culture also displayed reduced

proliferation inhibition (AUC_{pi} and max. PI) induced by gemcitabine (Fig. 2C and D). For 5-FU, only a slight but significant decrease in max. PI was observed. No significant difference was found in organoid proliferation inhibition in the presence of CAFs after paclitaxel treatment (Fig. 2C and D). Worth noting, paclitaxel was less effective at inhibiting organoid proliferation than gemcitabine or 5-FU (Fig. 2C, AUC_{pi} values).

CAFs themselves showed almost no proliferation in 3D co-cultures (Supplementary Fig. S1F, control). Only 5-FU treatment induced a significant increment in CAF death levels ($P < 0.05$; Supplementary Fig. S1G).

In sum, our results show that CAFs exert a protective effect against the cytotoxic effects of gemcitabine, 5-FU and paclitaxel on PDAC-PDOs, indicating a direct contribution to tumor cell drug resistance. These results further highlight the relevance of heterotypic culture models for personalized in vitro drug testing.

Increased expression of inflammatory pathways in CAFs co-cultured with PDAC organoids

To gain insight into the mechanisms behind the increased chemoresistance of PDAC organoids triggered by CAFs, we performed scRNA-seq to identify transcriptional changes induced in PDO/CAF co-cultures. Three pairs of organoids and patient-matched CAFs (lines 100, 107 and 112) were sequenced after 5 days in 3D mono- and co-culture (Fig. 3A). A total of 13,235 PDAC cells and 7,356 CAFs were sequenced and analyzed (Supplementary Fig. S2A and B). Organoid cells were identified by the expression of the tumor markers KRT18 and KRT19 whereas CAFs were characterized by DCN and LUM expression (Fig. 3B). Patient-specific clustering was observed for organoids and CAF populations, indicating transcriptional heterogeneity between the individual samples (Fig. 3B).

Clustering of all sequenced CAFs distinguished seven transcriptional clusters (Fig. 3C, D and Supplementary Fig. S2C), with distinct functional identities, as indicated by functional enrichment analysis for gene ontology (GO) terms. The largest cluster, cluster 0, was functionally characterized by expression of genes related

(See figure on next page.)

Fig. 1 Co-culture of PDAC organoids with CAFs and image-based drug testing to de-convolve CAF and organoid responses. **A** Brightfield images corresponding to the five established direct 3D co-cultures of the patient-matched CAFs and PDAC-PDOs. Scale bar: 250 μ m. **B** Co-culture of matched CAFs and PDAC-PDOs stained for the CAF marker α -SMA (red) and actin cytoskeleton (phalloidin, green). Nuclei were stained with Hoechst (blue). Direct intercellular contact between organoid tumor cells and CAFs can be observed. Scale bar: 50 μ m. **C** Proliferation levels of PDAC organoids measured from culture day 3 to day 8. PDAC organoids in co-culture show significantly higher proliferation levels than in monoculture. Paired t-test, * $P < 0.05$. **D** Schematic overview of the established drug test workflow for PDAC-PDO mono- and PDAC-PDO/CAF co-cultures. **E** Montage of maximum intensity projections as an example of the image data generated from a co-culture model treated with increasing concentration of 5-FU. CAFs (blue) were stained with CellTracker Green CMFDA to be distinguished from PDAC organoids. Hoechst (green) and propidium iodide (red) were used to stain the nuclei of all and dead cells, respectively. **F** Dose-response curves for cell death (left) and proliferation (right) were computed individually for PDOs and CAFs. Area under the curve (AUC, AUC_{pi}) and maximum response values (max. Death, max. PI) for cell death and proliferation inhibition were used to evaluate drug responses

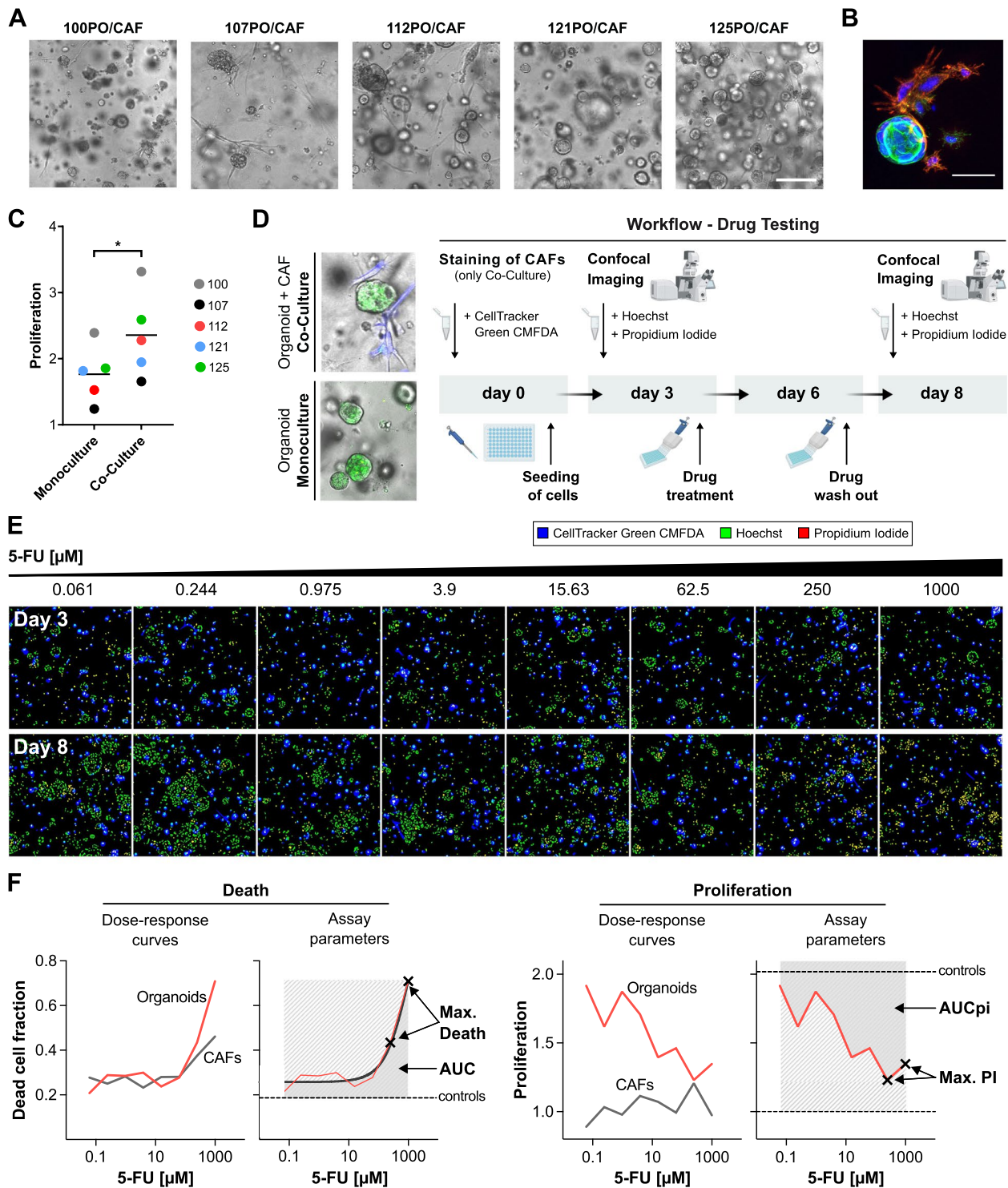


Fig. 1 (See legend on previous page.)

to extracellular matrix and epithelial to mesenchymal transition. In co-culture, we observed an increase in the proportion of CAFs from cluster 5 (Fisher's exact test,

$p < 0.0001$; Fig. 3E), which was characterized by a higher expression of genes related to cell cycle, suggesting a potential increase of CAF proliferation in co-culture. This

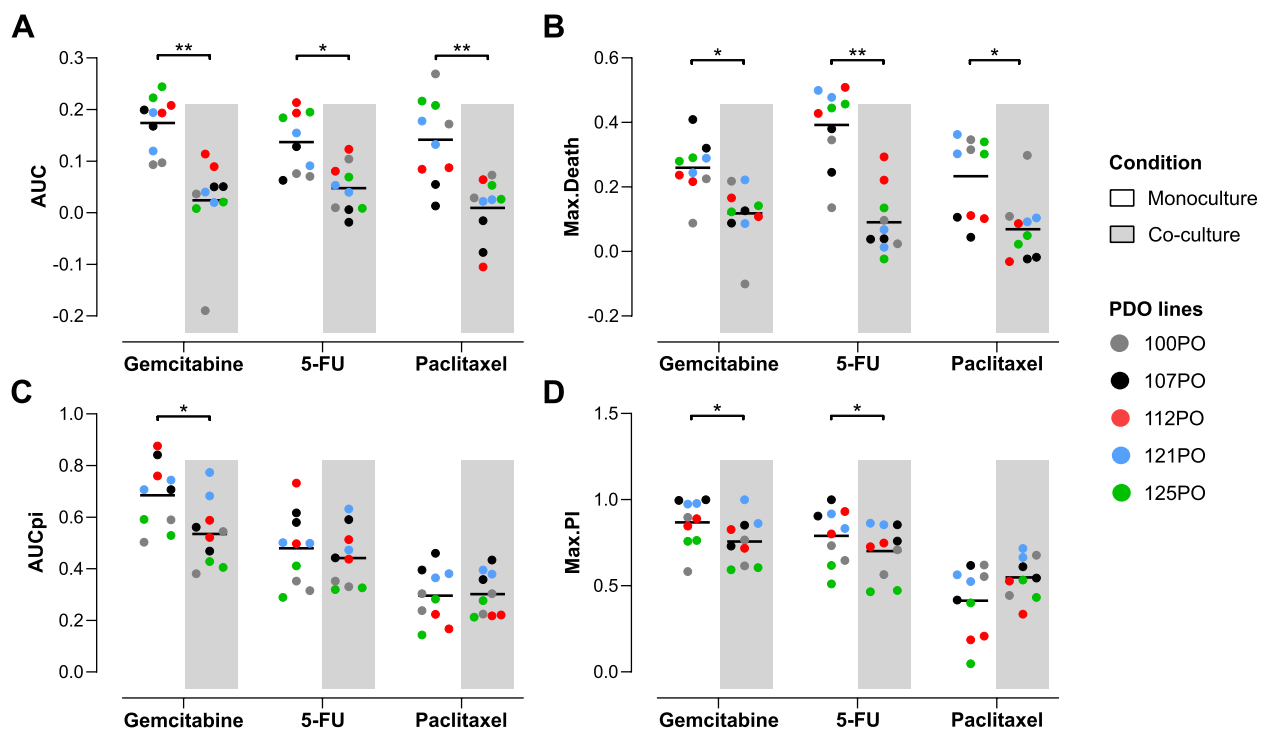


Fig. 2 Decreased drug sensitivity of organoids in co-culture with matched CAFs. **A, B** Cell death of PDAC organoids induced by gemcitabine, 5-FU and paclitaxel was significantly reduced when co-cultured with CAFs. The mean values of the two independent replicates for each line are displayed. Paired t-test, * $P < 0.05$, ** $P < 0.01$. **C, D** Proliferation inhibition induced by gemcitabine in PDAC organoids was significantly reduced in co-culture (AUCpi, max. PI). For 5-FU, a significantly lower max. PI was observed for PDAC organoids in co-culture. The mean values of the two independent replicates for each line are displayed. Paired t-test, * $P < 0.05$

increase was consistent across all three patient samples (Supplementary Fig. S2C). On the other hand, contribution of cluster 1, related to inflammation, locomotion and TNF- α signaling, decreased in co-culture (Fisher's exact test, $p < 0.0001$; Fig. 3E), although this was restricted to case 112 at the individual sample level (Supplementary Fig. S2C). However, we note that these proportions based on scRNA-seq data may not fully reflect cell numbers in cultures, due to possible differences in dissociation efficiency between CAF subtypes.

The two CAF subtypes previously described [20], myCAFs and iCAFs, were identified as CAF subpopulations. Principal component analysis on iCAF and myCAF marker genes [27] for all sequenced CAFs resolved 2 distinct transcriptional clusters (Supplementary Fig. S2D). 88.5% of the CAF population corresponded to myCAFs (6509 cells), whereas 11.5% were classified as iCAFs (847 cells). iCAFs corresponded almost exclusively to the inflammation-related cluster 1 (Fig. 3F). Expression levels of iCAF marker genes were higher in the co-culture setting than in monocultures (Fig. 3G).

We further compared CAFs in mono- and co-culture by gene set enrichment analysis of differentially expressed genes across all cell clusters. Two of the significantly

enriched gene sets in co-culture were associated with proliferation (REACTOME_CELL_CYCLE, HALLMARK_E2F_TARGETS; Fig. 3H), which is in line with the increased proportion of the cell cycle related cluster 5. Remarkably, among the top enriched gene sets in co-culture we found hallmark gene sets related to inflammation (TNF α signaling via NF κ B, interferon gamma and alpha responses and TGF β signaling, Fig. 3H and I).

Altogether, these results indicate that co-culture with PDAC organoids induces a pro-inflammatory phenotype in CAFs, which might drive the enhanced chemo-resistance in tumor cells and could be amenable to molecular targeting.

PDAC organoids display increased expression of EMT genes in 3D co-culture with CAFs

Eight transcriptional clusters were identified for all sequenced PDAC-PDO cells (Fig. 4A, B, Supplementary Fig. S3B and C). The proportion of each cluster differed between organoid lines, reflecting patient-specific transcriptional heterogeneity. For instance, cluster 0, characterized by expression of genes related to adhesion and cell junctions, was the predominant cluster of line 100PO, whereas the immune response related cluster 1

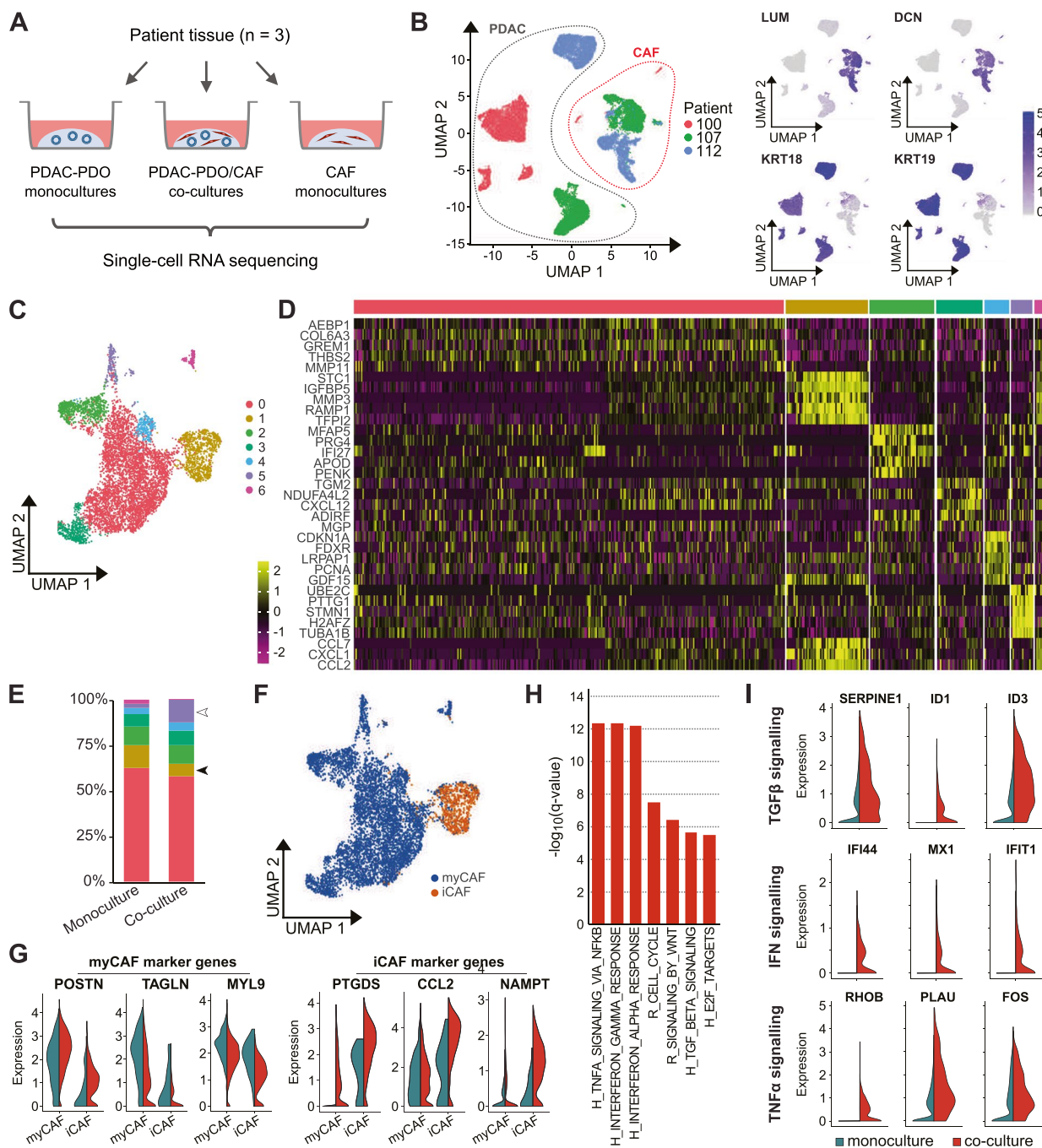


Fig. 3 Inflammatory pathways are upregulated in CAFs after co-culture with PDAC organoids. **A** Overview of the samples used for single-cell RNA sequencing. **B** UMAP representation of all single-cell transcriptomes. Dotted lines indicate CAF and PDAC cells, which were distinguished by the expression of known marker genes. LUM and DCN expression identifies CAFs, while KRT18 and KRT19 expression identifies PDAC tumor cells. **C** Integrated UMAP representation of CAFs from monoculture and co-culture samples, with seven clusters distinguished by Louvain clustering. **D** Single-cell expression of the top five enriched genes for each CAF cluster in monoculture and co-culture samples, with seven clusters distinguished by Louvain clustering. **E** Distribution of CAFs among the seven clusters, colored as in (C), in monoculture and co-culture samples. The proportion of cells in cluster 1, with an immune response signature, is decreased in co-cultures (filled arrowhead); the proportion of cells in cluster 5, expressing cell cycle related genes, is increased in co-cultures (unfilled arrowhead). **F** Distribution of iCAF-like and myCAF-like cells, as identified by principal component analysis (Methods and Supplementary Fig. S2D), shown on the same UMAP as in (C). **G** Expression of iCAF and myCAF marker genes in the iCAF-like and myCAF-like populations identified in (F), comparing monocultures (blue) to co-cultures (red). **H** Selected Hallmark (H) and Reactome (R) pathways upregulated in CAFs in co-cultures compared to monocultures. **I** Expression of genes involved in TGFB β , IFN and TNF α signaling in CAFs in monocultures (blue) and co-cultures (red) showing increased expression of genes in co-culture conditions

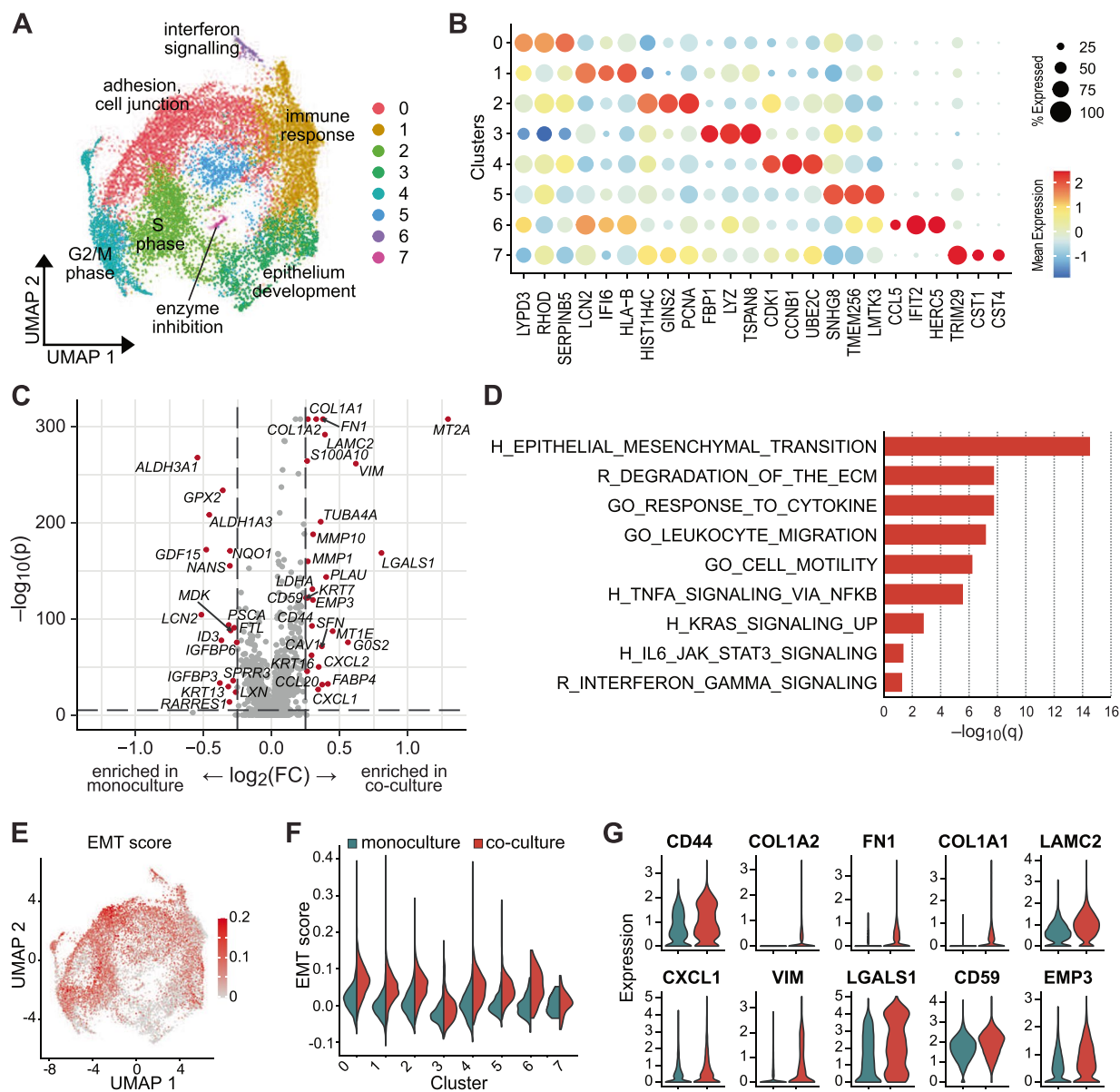


Fig. 4 Increased EMT in PDAC organoid cells induced by CAFs. **A** Integrated UMAP representation of PDAC organoid cells from monoculture and co-culture samples, with eight clusters distinguished by Louvain clustering. Keywords indicate functional cluster identities based on GO term analysis. **B** Expression across all PDAC organoid clusters of genes specifically enriched in one cluster. **C** Volcano plot depicting the fold change and significance of genes differentially expressed in PDAC organoid cells in monocultures compared to co-cultures. **D** Selected Hallmark (H), Reactome (R) and GO gene sets upregulated in PDAC organoid cells in co-cultures compared to monocultures. **E** Distribution of EMT scores in PDAC organoid cells, using the same UMAP representation as in (A). **F** Distribution of EMT scores by cluster in PDAC organoid cells in monocultures (blue) and co-cultures (red). **G** Expression of EMT-related genes in PDAC organoid cells in monocultures (blue) and co-cultures (red)

represented most cells in line 107PO (Supplementary Fig. S3A). No predominant cluster was identified in line 112PO (Supplementary Fig. S3A). Interestingly, we did not observe significant changes in the proliferation score for any of the identified transcriptional clusters

of PDAC organoid cells in co-culture compared with monoculture (Supplementary Fig. S3D).

We further characterized PDO cells in terms of the two major transcriptional subtypes in PDAC, namely classical and basal-like subtypes, by scoring the expression of each subtype gene signatures at the single-cell level. Organoid

line 100PO comprised predominantly cells with higher basal-like scores, whereas 107PO and 112PO showed higher classical scores (Supplementary Fig. S3E). No significant differences in the subtype scores were observed between mono- and co-culture conditions, indicating that the presence of CAFs did not induce a shift in the subtype state of the tumor cells in our model (Supplementary Fig. S3E and F).

To assess the transcriptional changes induced by co-culture with CAFs, we analyzed the differentially expressed genes between PDAC organoid cells in mono- and co-culture conditions (Fig. 4C). Several genes associated with epithelial-to-mesenchymal transition such as COL1A1, COL1A2, FN1, LAMC2 and VIM were upregulated in co-cultured organoid cells. Consistently, Gene Set Enrichment Analysis (GSEA) identified HALLMARK_EPITHELIAL_MESENCHYMAL_TRANSITION as the most significantly enriched gene set in the co-culture settings (Fig. 4D). Additionally, gene sets associated with inflammation such as HALLMARK_TNFA_SIGNALING_VIA_NFKB, HALLMARK_IL6_JAK_STAT3_SIGNALING or REACTOME_INTERFERON_GAMMA_SIGNALING were also found to be enriched in organoid cells co-cultured with CAFs.

Further focusing on the EMT signature of the identified transcriptional clusters of PDAC cells, we found an increased EMT expression score for almost all clusters in co-culture conditions (Fig. 4E and F), consistent with the result of the GSEA. Expression of several individual EMT-related genes was also upregulated in co-culture (Fig. 4G). Using CellPhoneDB, an open repository of ligand-receptor interactions [32], we were able to detect potential intercellular receptor-ligand interactions between PDO cells (receptor) and CAFs (ligand) (Fig. 5A). In general, most interactions took place between organoid cells in cluster 0 and CAFs. Since cluster 0 was characterized by genes involved in adhesion and cell junctions, this suggests direct intercellular interactions. Additionally, several receptor-ligand interactions related to EMT were identified between PDAC organoid cells and CAFs (Fig. 5B) such as CD44-HGF, CD44-LGALS9 or CD44-FGF2. Most of these EMT-related interactions occurred between CAFs and PDAC organoid cells in cluster 0 as well as clusters 2 and 4 representing cycling PDAC cells (2: S-Phase, 4, G2/M-Phase). Spatial proximity and co-localization of the receptor-ligand interaction pair CD44-HGF could be confirmed in the original tissues by immunofluorescence staining (Fig. 5C), supporting the *in vivo* relevance of tumor-stroma interactions occurring in our co-culture model.

Taken together, these findings indicate that intercellular interactions between CAFs and epithelial cancer cells are reproduced in our co-culture system, leading

to the upregulation of EMT in PDAC organoid cells and increased chemoresistance.

Discussion

Initial studies have demonstrated that PDAC organoids reflect the genetic diversity of the original tumors and that drug sensitivity of organoid lines correlates with clinical response, providing a first indication of their potential for personalized medicine [16, 19]. However, the absence of stromal components in these models has not yet allowed to evaluate the influence of stromal activity and signaling on chemosensitivity and precludes screening of drugs targeting stromal elements or tumor-stroma interactions.

In this study, we established direct co-cultures of patient-matched PDAC organoids and CAFs and showed that CAFs promoted epithelial cancer cell proliferation as well as resistance of cancer cells to gemcitabine, 5-FU and paclitaxel. The use of the image-based DeathPro assay [22] allowed us to overcome the challenge of differentiating cell type-specific drug responses. Common *in vitro* viability assays such as MTT or CellTiter Glo are not capable of differentiating drug responses of stromal and tumor cells when directly co-cultured. Hence, in addition to discerning specific tumor cell responses, this system allows monitoring the specific effect of drug treatment on CAFs, providing an excellent tool to study combination therapies targeting tumor and stromal cells.

Previous studies have reported enhanced chemoresistance of primary human PDAC cells in the presence of unmatched stromal cells in 3D tumor spheroid and bioengineered models [35, 36]. Similarly, Tsai et al. reported an increase in IC50 after gemcitabine treatment of one patient-derived organoid line in co-culture with CAFs [21]. Our work extends on these observations in a patient-specific manner, highlighting the feasibility and relevance of complex organoid models for *ex vivo* drug response prediction in the clinical setting. In our scRNA-seq data, we observed unsupervised clustering of organoid tumor cells as well as of CAFs by patient of origin; patient-specific heterogeneity is thus preserved in both cell populations. These results accentuate the need and potential to incorporate patient-matched stromal cells into organoids to faithfully model tumor diversity across patients. In our experience, the limiting factor for clinical application of our co-culture model would be the time necessary to reach sufficient purity and biomass of the organoid cultures. Successful establishment and expansion of organoid lines was accomplished in 50% of the cases and downstream applications could be performed after a median of 40 days. Considering that adjuvant therapy is commonly started between 6 and 12 weeks after resection, drug response prediction based on our model

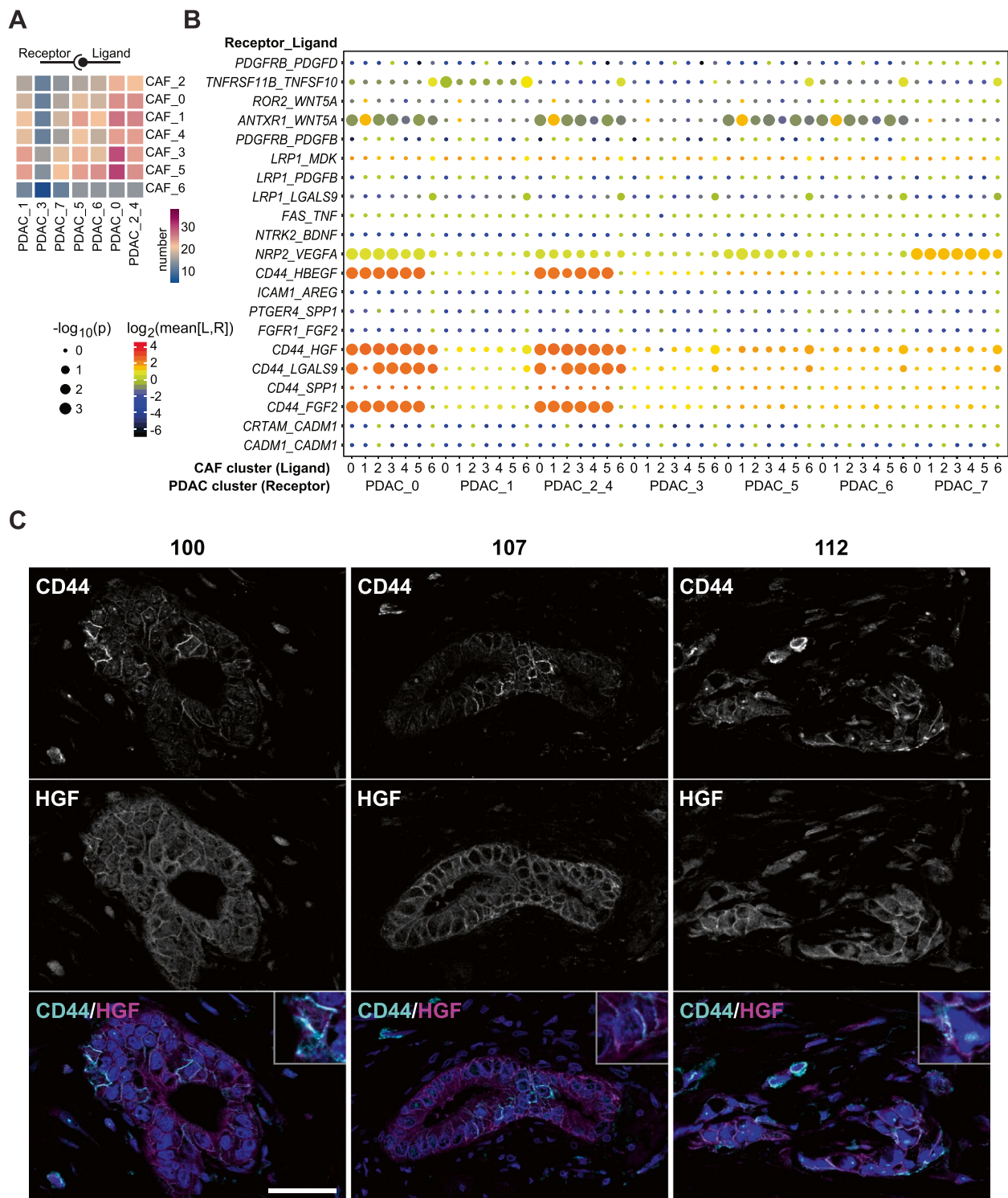


Fig. 5 Potential receptor-ligand interactions between PDAC organoids and CAFs. **A** Number of potential ligand-receptor interactions between the different CAF and PDAC organoids cell clusters. **B** Potential receptor-ligand interactions between PDAC organoid and CAF cell clusters with a known or presumed role in EMT. Shown are only interactions where CAF cells present a ligand to the receptor expressed by PDAC organoid cells. **C** Immunofluorescence staining for CD44 (cyan) and HGF (magenta) of the parental tumor tissues of PDO/CAF lines 100, 107 and 112 confirms co-localization of a predicted receptor-ligand interaction in vivo. Single channels and composite are shown. DAPI stained nuclei are depicted in blue. Scale bar: 50 μ m

could inform first-line adjuvant treatment for a subset of patients while results could be available to inform second-line treatments for most of these patients. Additionally, successful generation of PDAC-PDOs [18, 38, 39] as well as a PDO/CAF pair [37] from minimal samples such as fine-needle biopsies have been previously reported, supporting a potential clinical application in the neoadjuvant or palliative settings. Further optimization and patient-specific tailoring of organoid culture conditions to accelerate organoid expansion could be therefore highly beneficial. Recently, Harryvan et al. [37] described a pancreatic mini-tumor model established from patient-derived organoids and CAFs, which was able to model the characteristic desmoplastic reaction observed in PDAC tumors. In their study, CAF activation and proliferation was induced by activation of transforming growth factor and platelet-derived growth factor β signaling pathways via modulation of culture media components, supporting the potential of fine-tuning PDO/CAF co-culture conditions to model even more closely tumor drug response.

Our scRNA-seq analyses also revealed transcriptional changes towards an EMT phenotype in co-cultured organoid cells, consistent with the results reported by Ligorio and colleagues for 2D co-cultures of patient-derived PDAC cell lines derived from metastatic ascites and unmatched CAFs [40]. This observation is also in line with previous reports of EMT induction in PDAC cell lines after indirect co-culture with pancreatic stellate cells (PSCs) cells [41] or exposure to PSC-condition medium [42]. In vivo, orthotopically grafted human organoids surrounded by a stromal microenvironment evidenced upregulation of EMT signaling relative to organoids engrafted intraductally, emphasizing that induction of EMT in tumor cells by the stromal microenvironment is a relevant process in vivo [43]. While the role of EMT in driving PDAC chemoresistance is widely recognized [44, 45], our results indicate CAF-mediated induction of EMT in organoids as one of the mechanisms contributing to their chemo-protectant effect in our co-culture system.

Despite changes in EMT, we did not observe shifts in the transcriptional subtype signatures of the tumor cells under our culture conditions. Although proliferation of organoids was enhanced in co-cultures, proliferation scores derived from the scRNA-seq analyses were not significantly different between mono- and co-cultures. Similarly, the increment in the proportion of the CAF cluster expressing cell cycle related genes observed in co-cultures was not accompanied by enhanced CAF proliferation as determined by Death-Pro. It is worth noting that in our scRNA-seq data we identified considerably lower numbers of CAFs in co-culture compared to CAF monoculture samples. It

is thus conceivable that the observed changes in CAF cluster proportions might be due to differential loss of CAF cells in the co-culture setting during sample processing due to, for example, preferential survival of cells with rounded shape or exclusion of CAF-tumor cell doublets. A challenging recovery of CAFs has also been reported for primary pancreatic tumor samples [27], raising awareness that single cell analyses of CAFs might be generally affected by technical biases during dissociation.

Depletion of tumor stroma results in more aggressive tumors and reduced survival in preclinical models [46, 47] and stroma-depleting agents have shown no benefit in clinical trials [48]. Targeting of specific tumor-stromal cells interactions, in contrast, has become a promising therapeutic approach for PDAC [49]. Results from our scRNA-seq analyses identified several potential interactions involving the cancer stem cell marker CD44 with ligands secreted by CAFs such as HGF, HBEGF, FGF2 and LGALS9. We could also show colocalization of CD44 and HGF in the parental tumor tissues, validating the relevance of predicted interactions from our co-culture model in the in vivo context. CD44 signaling has also been shown to promote stemness via a SPP1-CD44 axis [50] and high expression of CD44 has been associated with poor prognosis in PDAC [51]. Evidence from patient-derived xenografts shows that CD44⁺ cells are the source of PDAC relapse after gemcitabine treatment, rendering CD44 a promising therapeutic target against recurrent disease [52].

Conclusions

Altogether, our study demonstrates increased chemoresistance of PDAC organoids in co-culture with patient-matched CAFs, emphasizing the relevance of complex co-culture models for personalized medicine applications. This also opens the possibility to investigate efficacy and mode of action for drugs targeting the tumor microenvironment in a patient-specific manner. Hence, our work provides evidence of the feasibility of modeling patient-specific tumor-stroma interactions for target discovery and drug testing in a high-throughput amenable 3D culture setting.

Abbreviations

CAFs	Cancer-associated fibroblasts
PDAC	Pancreatic ductal adenocarcinoma
3D	Three dimensional
EMT	Epithelial-to-mesenchymal transition
ECM	Extracellular matrix
PDOs	Patient-derived PDAC organoids
5-FU	5-fluorouracil

scRNA-seq	Single cell RNA-sequencing
iCAFs	Inflammatory CAFs
myCAFs	Myofibroblastic CAFs
AUC	Area under the curve
PI	Proliferation inhibition
GSEA	Gene Set Enrichment Analysis
PSCs	Pancreatic stellate cells

Supplementary Information

The online version contains supplementary material available at <https://doi.org/10.1186/s13046-022-02519-7>.

Additional file 1 : Supplementary Figures. Supplementary Figs. S1 to S3.

Additional file 2 : Supplementary Table S1. Additional information of scRNA-seq data: maximum number of counts per gene and a maximum fraction of mitochondrial reads.

Acknowledgments

We acknowledge support from the Biobank of the European Pancreas Centre at the Department of General and Visceral Surgery of the University Hospital (EPZ-Pancobank), working in accordance with the regulations of the tissue banks and upon an approval of the Ethics Committee of Heidelberg University (Ethic votes S-708/2019 and S-083/2021). Collection & processing of the samples and clinical data by the EPZ-Pancobank was supported by the Heidelberger Stiftung Chirurgie and in part by the German Ministry of Science and Education (BMBF) grants 01ZX1305C, 01ZX1605C, 01KT1506. The EPZ-Pancobank is a member of the BioMaterial Bank Heidelberg (supervisor: Prof. P. Schirmacher, BMBF grant# 01EY1101 and GBA/BBMRI.de grant 01EY1707) belonging to the German Biobank Alliance. We thank the group of Prof. B. Messner (MUW) for the helpful technical support with immunofluorescence staining. We thank K. Felix for helpful discussions. We thank K. Schneider, E. Lederer, K. Ruf and M. Fischer for the excellent technical support.

Authors' contributions

SS planned, performed all experiments and analyzed data. SLB planned, supported and supervised experiments and wrote the original manuscript with support from SS. JJ planned, performed experiments and analyzed data. TGK performed bioinformatic data analysis. MS and NAG contributed with tissue sample acquisition and clinical data. RE and MWB acquired funding and provided scientific and infrastructural support. OS and CC conceived the project, analyzed data, acquired funding and provided supervision. All authors read and approved the final manuscript.

Funding

This work received financial support from NCT 3.0 Extension Programm (NCT3.0_2015.17 PrecO-Panc) and PANC-STRAT - single cell sequencing extension (BMBF 01ZX1605C). S.L.B. and O.S. were supported by the National Center of Tumor Diseases (NCT) Heidelberg (NCT3.0_2015.17 PrecO-Panc). Open Access funding enabled and organized by Projekt DEAL.

Availability of data and materials

Single-cell sequencing data will be deposited at the European Genome-Phenome Archive (EGA) under accession number EGAS00001006661. All materials will be available upon request through a material transfer agreement.

Declarations

Ethics approval and consent to participate

All patient material and clinical information was obtained from the Biobank of the European Pancreas Centre at the Department of General and Visceral Surgery of the University Hospital Heidelberg (EPZ-Pancobank) under the ethic votes 301/2001, 159/2002, S-206/2011, S-708/2019 and S-083/2021 approved by the ethical committee of University of Heidelberg. All patients provided written informed consent.

Consent for publication

Not applicable.

Competing interests

J. Jabs was employed by DKFZ and Steinbeis GmbH during experimental work and analysis and at Merck Healthcare KGaA during writing of the manuscript. All other authors declare no conflict of interest.

Author details

¹European Pancreas Center, Department of General Surgery, University Hospital Heidelberg, Heidelberg, Germany. ²Division of Molecular Oncology of Gastrointestinal Tumors, German Cancer Research Center (DKFZ), Heidelberg, Germany. ³NCT partner site Heidelberg, a clinical-translational cancer research partnership between University Hospital Heidelberg and DKFZ, Heidelberg, Germany. ⁴Division of Visceral Surgery, Department of General Surgery, Medical University of Vienna, Vienna, Austria. ⁵Berlin Institute of Health at Charité – Universitätsmedizin Berlin, Digital Health Center, Berlin, Germany. ⁶Division of Theoretical Bioinformatics, German Cancer Research Center (DKFZ), Heidelberg, Germany. ⁷Present Address: Merck Healthcare KGaA, Global Research, Darmstadt, Germany.

Received: 17 June 2022 Accepted: 12 October 2022

Published online: 22 October 2022

References

1. Ferlay J, Ervik M, Lam F, Colombet M, Mery L, Piñeros M, et al. Global Cancer Observatory: Cancer Today. Lyon, France: International Agency for Research on Cancer. 2020 [cited 2022 Mar 7]. Available from: <https://gco.iarc.fr/today>
2. Springfield C, Jäger D, Büchler MW, Strobel O, Hackert T, Palmer DH, et al. Chemotherapy for pancreatic cancer. *La Press Médicale*. 2019;48:e159–74.
3. Klemm F, Joyce JA. Microenvironmental regulation of therapeutic response in cancer. *Trends Cell Biol*. 2015;25:198–213.
4. Kleeff J, Korc M, Apte M, Vecchia CL, Johnson CD, Biankin AV, et al. Pancreatic cancer. *Nat Rev Dis Primers*. 2016;2:16022.
5. Olive KP, Jacobetz MA, Davidson CJ, Gopinathan A, McIntyre D, Honess D, et al. Inhibition of hedgehog signaling enhances delivery of chemotherapy in a mouse model of pancreatic cancer. *Science*. 2009;324:1457–61.
6. Provenzano PP, Cuevas C, Chang AE, Goel VK, Von Hoff DD, Hingorani SR. Enzymatic targeting of the stroma ablates physical barriers to treatment of pancreatic ductal adenocarcinoma. *Cancer Cell*. 2012;21:418–29.
7. Biffi G, Tuveson DA. Diversity and biology of cancer-associated fibroblasts. *Physiol Rev*. 2021;101:147–76.
8. Huanwen W, Zhiyong L, Xiaohua S, Xinyu R, Kai W, Tonghua L. Intrinsic chemoresistance to gemcitabine is associated with constitutive and laminin-induced phosphorylation of FAK in pancreatic cancer cell lines. *Mol Cancer*. 2009;8:125.
9. Ireland L, Santos A, Ahmed MS, Rainer C, Nielsen SR, Quaranta V, et al. Chemoresistance in pancreatic cancer is driven by stroma-derived insulin-like growth factors. *Cancer Res*. 2016;76:6851–63.
10. Hesler RA, Huang JJ, Starr MD, Treboschi VM, Bernanke AG, Nixon AB, et al. TGF- β -induced stromal CYR61 promotes resistance to gemcitabine in pancreatic ductal adenocarcinoma through downregulation of the nucleoside transporters hENT1 and hCNT3. *Carcinogenesis*. 2016;37:1041–51.
11. Dalin S, Sullivan MR, Lau AN, Grauman-Boss B, Mueller HS, Kreidl E, et al. Deoxycytidine release from pancreatic stellate cells promotes gemcitabine resistance. *Cancer Res*. 2019;79:5723–33.
12. Richards KE, Zeleniak AE, Fishel ML, Wu J, Littlepage LE, Hill R. Cancer-associated fibroblast exosomes regulate survival and proliferation of pancreatic cancer cells. *Oncogene*. 2017;36:1770–8.
13. Hutchinson L, Kirk R. High drug attrition rates—where are we going wrong? *Nat Rev Clin Oncol*. 2011;8:189–90.
14. Boj SF, Hwang C-I, Baker LA, Chio IIC, Engle DD, Corbo V, et al. Organoid models of human and mouse ductal pancreatic cancer. *Cell*. 2015;160:324–38.

15. Tiriach H, Belleau P, Engle DD, Plenker D, Deschênes A, Somerville T, et al. Organoid profiling identifies common responders to chemotherapy in pancreatic cancer. *Cancer Discov*. 2018;8:1112–29.
16. Le Blanc S, Ishaque N, Jabs J, Bauer T, Schuth S, Hu Q, et al. Deep molecular characterization linked to drug response profiling of pancreatic ductal adenocarcinoma using patient-derived organoids. *Biorxiv*. 2021; 2021.08.26.457743.
17. Driehuis E, Hoeck A van, Moore K, Kolders S, Francies HE, Gulersonmez MC, et al. Pancreatic cancer organoids recapitulate disease and allow personalized drug screening. *Proc National Acad Sci* 2019;116:26580–26590.
18. Seppälä TT, Zimmerman JW, Sereni E, Plenker D, Suri R, Rozich N, et al. Patient-derived organoid pharmacotyping is a clinically tractable strategy for precision medicine in pancreatic cancer. *Ann Surg*. 2020;272:427–35.
19. Grossman JE, Muthuswamy L, Huang L, Akshinthala D, Perea S, Gonzalez RS, et al. Organoid sensitivity correlates with therapeutic response in patients with pancreatic cancer. *Clin Cancer Res Official J Am Assoc Cancer Res*. 2022;28:708–18.
20. Öhlund D, Handly-Santana A, Biffi G, Elyada E, Almeida AS, Ponz-Sarvise M, et al. Distinct populations of inflammatory fibroblasts and myofibroblasts in pancreatic cancer. *J Exp Med*. 2017;214:579–96.
21. Tsai S, McOlash L, Palen K, Johnson B, Duris C, Yang Q, et al. Development of primary human pancreatic cancer organoids, matched stromal and immune cells and 3D tumor microenvironment models. *BMC Cancer*. 2018;18:335.
22. Jabs J, Zickgraf FM, Park J, Wagner S, Jiang X, Jechow K, et al. Screening drug effects in patient-derived cancer cells links organoid responses to genome alterations. *Mol Syst Biol*. 2017;13:955 Available from: <https://www.ncbi.nlm.nih.gov/pubmed/29180611>.
23. Bachem MG, Schneider E, Groß H, Weidenbach H, Schmid RM, Menke A, et al. Identification, culture, and characterization of pancreatic stellate cells in rats and humans. *Gastroenterology*. 1998;115:421–32.
24. Conrad C, Wunsche A, Tan TH, Bulkescher J, Sieckmann F, Verissimo F, et al. Micropilot: automation of fluorescence microscopy-based imaging for systems biology. *Nat Methods*. 2011;8:246–9.
25. Krieger TG, Le Blanc S, Jabs J, Ten FW, Ishaque N, Jechow K, et al. Single-cell analysis of patient-derived PDAC organoids reveals cell state heterogeneity and a conserved developmental hierarchy. *Nat Commun*. 2021;12:5826.
26. Stuart T, Butler A, Hoffman P, Hafemeister C, Papalexi E, Mauck WM, et al. Comprehensive integration of single-cell data. *Cell*. 2019;177:1888–1902.e21.
27. Elyada E, Bolisetty M, Laise P, Flynn WF, Courtois ET, Burkhart RA, et al. Cross-species single-cell analysis of pancreatic ductal adenocarcinoma reveals antigen-presenting cancer-associated fibroblasts. *Cancer Discov*. 2019;9:1102–23.
28. McInnes L, Healy J, Melville J. UMAP: uniform manifold approximation and projection for dimension reduction. *Arxiv*. 2018:1802.03426.
29. Subramanian A, Tamayo P, Mootha VK, Mukherjee S, Ebert BL, Gillette MA, et al. Gene set enrichment analysis: a knowledge-based approach for interpreting genome-wide expression profiles. *Proc Natl Acad Sci USA*. 2005;102:15545–50.
30. Liberzon A, Subramanian A, Pinchback R, Thorvaldsdóttir H, Tamayo P, Mesirov JP. Molecular signatures database (MSigDB) 3.0. *Bioinformatics*. 2011;27:1739–40.
31. Moffitt RA, Marayati R, Flate EL, Volmar KE, Loeza SGH, Hoadley KA, et al. Virtual microdissection identifies distinct tumor- and stroma-specific subtypes of pancreatic ductal adenocarcinoma. *Nat Genet*. 2015;47:1168–78.
32. Efremova M, Vento-Tormo M, Teichmann SA, Vento-Tormo R. Cell-PhoneDB: inferring cell–cell communication from combined expression of multi-subunit ligand–receptor complexes. *Nat Protoc*. 2020;15:1484–506.
33. Rashid NU, Peng XL, Jin C, Moffitt RA, Volmar KE, Belt BA, et al. Purity independent subtyping of tumors (PuriST), a clinically robust, single-sample classifier for tumor subtyping in pancreatic cancer. *Clin Cancer Res*. 2020;26:82–92.
34. Fontana F, Marzagalli M, Sommariva M, Gagliano N, Limonta P. In vitro 3D cultures to model the tumor microenvironment. *Cancers*. 2021;13:2970.
35. Firuzi O, Che PP, Hassouni BE, Buijs M, Coppola S, Löhr M, et al. Role of c-MET inhibitors in overcoming drug resistance in spheroid models of primary human pancreatic cancer and stellate cells. *Cancers*. 2019;11:638.
36. Osuna de la Peña D, Trabulo SMD, Collin E, Liu Y, Sharma S, Tatar M, et al. Bioengineered 3D models of human pancreatic cancer recapitulate in vivo tumour biology. *Nat Commun*. 2021;12:5623.
37. Harryvan TJ, Hawinkels LJAC, workgroup mini-tumor, Inderson A, van HJE, Micke P, et al. A novel pancreatic cancer mini-tumor model to study desmoplasia and MyCAF differentiation. *Gastro Hep Adv*. 2022;1:678–81.
38. Tiriach H, Bucobo JC, Tzimas D, Grewel S, Lacombe JF, Rowehl LM, et al. Successful creation of pancreatic cancer organoids by means of EUS-guided fine-needle biopsy sampling for personalized cancer treatment. *Gastrointest Endosc*. 2018;87:1474–80.
39. Lacombe JF, Plenker D, Tiriach H, Bucobo JC, D'souza LS, Khokhar AS, et al. Single-pass vs 2-pass endoscopic ultrasound-guided fine-needle biopsy sample collection for creation of pancreatic adenocarcinoma organoids. *Clin Gastroenterol H*. 2020;19:845–7.
40. Ligorio M, Sil S, Malagon-Lopez J, Nieman LT, Misale S, Pilato MD, et al. Stromal microenvironment shapes the Intratumoral architecture of pancreatic cancer. *Cell*. 2019;178:160–175.e27.
41. Kikuta K, Masamune A, Watanabe T, Ariga H, Itoh H, Hamada S, et al. Pancreatic stellate cells promote epithelial-mesenchymal transition in pancreatic cancer cells. *Biochem Biophys Res Commun*. 2010;403:380–4.
42. Wu YS, Chung I, Wong WF, Masamune A, Sim MS, Looi CY. Paracrine IL-6 signaling mediates the effects of pancreatic stellate cells on epithelial-mesenchymal transition via Stat3/Nrf2 pathway in pancreatic cancer cells. *Biochim Biophys Acta Gen Subj*. 2017;1861:296–306.
43. Miyabayashi K, Baker LA, Deschenes A, Traub B, Caligiuri G, Plenker D, et al. Intraductal transplantation models of human pancreatic ductal adenocarcinoma reveal progressive transition of molecular subtypes. *Cancer Discov*. 2020:CD-20-0133.
44. Zheng X, Carstens JL, Kim J, Scheible M, Kaye J, Sugimoto H, et al. EMT program is dispensable for metastasis but induces chemoresistance in pancreatic cancer. *Nature*. 2015;527:525–30.
45. Arumugam T, Ramachandran V, Fournier KF, Wang H, Marquis L, Abbruzzese JL, et al. Epithelial to mesenchymal transition contributes to drug resistance in pancreatic cancer. *Cancer Res*. 2009;69:5820–8.
46. Özdemir BC, Pentcheva-Hoang T, Carstens JL, Zheng X, Wu C-C, Simpson TR, et al. Depletion of carcinoma-associated fibroblasts and fibrosis induces immunosuppression and accelerates pancreas cancer with reduced survival. *Cancer Cell*. 2014;25:719–34.
47. Rhim AD, Oberstein PE, Thomas DH, Mirek ET, Palermo CF, Sastra SA, et al. Stromal elements act to restrain, rather than support, pancreatic ductal adenocarcinoma. *Cancer Cell*. 2014;25:735–47.
48. Kim EJ, Sahai V, Abel EV, Griffith KA, Greenson JK, Takebe N, et al. Pilot clinical trial of hedgehog pathway inhibitor GDC-0449 (Vismodegib) in combination with gemcitabine in patients with metastatic pancreatic adenocarcinoma. *Clin Cancer Res*. 2014;20:5937–45.
49. Nicolle R, Blum Y, Marisa L, Loncle C, Gayet O, Moutardier V, et al. Pancreatic adenocarcinoma therapeutic targets revealed by tumor-stroma cross-talk analyses in patient-derived xenografts. *Cell Rep*. 2017;21:2458–70.
50. Nallasamy P, Nimmakayala RK, Karmakar S, Leon F, Seshacharyulu P, Lakshmanan I, et al. Pancreatic tumor microenvironment factor promotes cancer stemness via SPP1–CD44 Axis. *Gastroenterology*. 2021;161:1998–2013.e7.
51. Franklin O, Billing O, Öhlund D, Berglund A, Herdenberg C, Wang W, et al. Novel prognostic markers within the CD44-stromal ligand network in pancreatic cancer. *J Pathology Clin Res*. 2019;5:130–41.
52. Molejon MI, Tellechea JI, Loncle C, Gayet O, Gilibert M, Duconseil P, et al. Deciphering the cellular source of tumor relapse identifies CD44 as a major therapeutic target in pancreatic adenocarcinoma. *Oncotarget*. 2015;6:7408–23.

Publisher's Note

Springer Nature remains neutral with regard to jurisdictional claims in published maps and institutional affiliations.